CHAPTER ONE HUNDRED FIFTY ONE

A THEORETICAL AND EXPERIMENTAL STUDY OF UNDERTOW

J. Buhr Hansen* and I. A. Svendsen*

ABSTRACT

It is well known that on a three-dimensional beach large volumes of water carried shorewards by the breakers feed longshore currents, which eventually escape back through the breaker line, often as rip currents.

In a steady two-dimensional situation, however, the mass flux represented by (among other things) the surface roller in the breakers returns as a seaward current close to the bottom. This current is called the undertow.

In this paper theoretical results for the undertow are compared with the results of recent laboratory experiments.

1. INTRODUCTION

Although known for years and described quite explicitly in texts on coastal morphology (see e.g Johnson 1919) the undertow seems for a long time to have escaped the attention of coastal engineers and scientists.

Undertow is the name used for the often very strong shore normal mean current which in a surf zone moves seaward below the level of the wave trough.

Clearly such a flow can only be maintained provided a similar flux of water is brought shorewards otherwise. This happens between crest and trough level in the broken surf zone waves. the situation is sketched in Fig. 1.

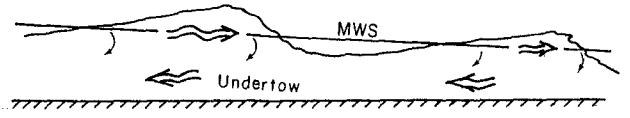

Fig. 1. The circulation flow in the vertical plane.

This circulation in the vertical plane represents a mechanism for maintaining the mass balance in the surf zone of a long beach. Another possible mechanism in the nearshore circulation is the three dimensional pattern of longshore and rip currents, which so far has received much more attention than the two dimensional circulation scheme in Fig. 1.

* Assoc. Prof., Institute of Hydrodynamics and Hydraulic Engineering (ISVA), Technical University of Denmark, DK-2800 Lyngby.

The purpose of the present paper is to discuss the physical processes responsible for the undertow. The discussion is supported by a theoretical model and recent laboratory measurements.

The undertow was observed experimentally by Bagnold (1940) and a qualitative analysis of the phenomenon was given by Dyhr-Nielsen and Sørensen (1970) in a descriptive paper which in essence contained most of the physical ideas pursued quantitatively in the following.

In the last few years the undertow has eventually attracted more attention. Thus Börekci (1982) presented a theoretical model based on the sinusoidal waves for the distribution over depth of this mean circulation, and an almost similar analysis was in fact given by Dally (1980).

Lately Louguet-Higgins (1983a,b) has considered several effects that may be caused by the strong pressure gradient from the set-up which also creates the undertow. In the last of the two papers in terms of convincing experimental demonstrations.

Finally Svendsen (1984b) presented a theoretical model based on the description of surf zone waves developed in Svendsen (1984a).

It may also be mentioned that laboratory values for the undertow can be extracted from the raw data of Stive and Winds experiments and were used by Svendsen (1984b). Also Guza (1984) reports that during the NSTS experiments at Californian beaches all current meters in the surf zone showed uniformly seaward going mean currents. This part of the data, however, has not been processed yet.

The theoretical model for the velocity profile of the undertow developed by Svendsen (1984b) differs from the models of Dally (1980) and Börekci (1982) in the way properties of the broken waves such as radiation stress and mass flux are determined.

The present paper will emphasize the physical aspects rather than mathematical details of the phenomenon, present some new measurements and also discuss the interaction with the bottom boundary layer, a point which was only briefly mentioned in Svendsen (1984b).

For several reasons an eulerian description has been chosen rather than a lagrangian. For one thing it is far simpler. Further all the measurements available are measurements at fixed points (i.e. eulerian descriptions). Most important, however, is the fact that the eulerian description is physically the more informative when mass balance, sedimenttransport etc. is considered.

2. THE MECANISM RESPONSIBLE FOR THE UNDERTOW

As mentioned in the introduction the undertow is a (strong) mean current which, superimposed on the oscillatory motion of the surf zone waves, moves seawards.

In this section is shown qualitatively that the undertow represents a balance between three equally important forces acting on the fluid particles.

For a start it is worth to recall that the turbulence created by the breakers spread downwards from the surface, where it was created, so that in the surf zone there is a substantial amount of turbulent kinetic energy present at all levels between bottom and surface. In such an environment a current like the undertow will generate large shear stresses which will tend to stop the current. Thus for the undertow to exist there must be a strong driving mechanism, which yields a seaward directed net force on each fluid particle.

It is well known that the depth- and time-averaged momentum balance

reads:

$$\frac{\partial S_{xx}}{\partial x} = -\rho g(h_o + b)\frac{\partial b}{\partial x} - \overline{\tau_b} \tag{2.1}$$

where b is the set-up, $\overline{\tau_b}$ is the mean bed shear stress, and the radiation stress S_{xx} is defined as

$$S_{xx} = \overline{\int_{-h}^{\eta+b} (\rho u^2 + p_D)dz} - \frac{1}{2}\rho g\overline{\eta^2} \tag{2.2}$$

The dynamic pressure p_D is defined by

$$p_D = \rho g(z-b) + p \tag{2.3}$$

In this balance, however, the individual contributions are not equally distributed over depth. In (2.2) both u and p will in general vary over the depth and, in surf zone waves in particular, by far the largest contributions to S_{xx} (including the last term in (2.2) come from the region between trough and crest.

The $\partial b/\partial x$ term in (2.1) on the other hand represents the pressure gradient from the sloping mean surface, and this contribution is the same at all z-levels. Fig. 2 shows the situation.

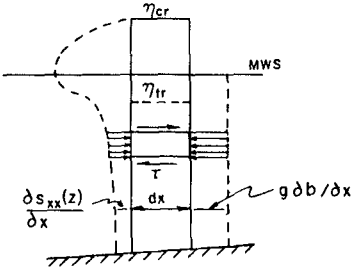

Fig. 2. The distribution of radiation stress and pressure gradients.

Consequently, if we consider a small fluid element at any z-level below trough level there will (in average over a wave period) be a net (seaward-directed) horizontal force on that fluid element equal to the difference between the local S_{xx}-contribution and $g\,\partial b/\partial x$. It is this net force which is driving the undertow. In Fig. 2 is also indicated the turbulent shear stress gradients which are responsible for preventing the current from accelerating indefinitely.

Thus a steady undertow establishes a balance between essentially three different forces: the radiation stress the pressure gradient due to set-up and the turbulent shear stresses created by the vertical variation of the undertow velocity in combination with the turbulence already present due to the breaking. The model used in the following is based on this balance. In principle it assumes (in addition to a situation steady in time) uniform conditions at different points in the shore normal direction. Since the depth varies this is clearly not quite true, but applies well to a gently sloping beach. The assumption corresponds to neglecting the convective accelerations in the shore normal direction, and on a steep beach this may not be acceptable.

3. THEORETICAL DESCRIPTION

From the description in Section 2 we realize that the undertow is associated with the strong set-up caused by wave breaking. Hence a proper quantitative description requires that the relevant characteristics of the surf zone waves are modeled suitably (see Svendsen, 1984a).

One of the important features is the mass or volume transport Q_s which occurs between crest and trough in the waves. Q_s is defined as (for definition of nomenclature see Fig. 3)

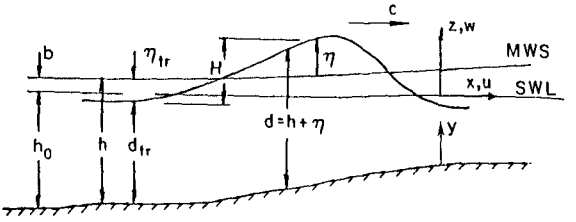

Fig. 3. Definition sketch.

$$Q_s = \overline{\int_{\eta_{tr}+b}^{\eta+b} u \, dz} \tag{3.1}$$

where $\overline{\quad}$ indicates average over a wave period.

In broken waves this is found to be composed of two contributions (Svendsen, 1984a): one is the ordinary effect of non-linearity known from non-breaking waves. The other is caused by the surface roller which is equivalent to an amount of water directly following the wave as it propagates shorewards. Thus the average particle velocity in the roller equals the progagation speed c of the wave.

It is therefore assumed that the velocity variation in the waves can be approximated as shown in Fig. 4.

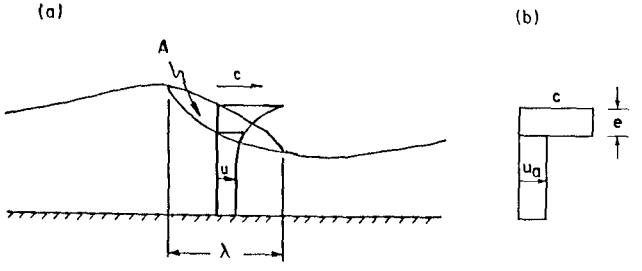

Fig. 4. a. Velocities in a breaker.
b. Velocity profile used in this paper.

This is combined with the assumption that the change in shape of the waves can be neglected locally which implies that

$$I \equiv \int_{-h_0}^{\eta+b} u \, dz = c\eta \tag{3.2}$$

As written (3.2) also presumes that there is no net mass flux in the waves (two dimensional problem), and that $\bar{\eta} = 0$ as indicated in Fig. 3.

When substituting these assumptions into (3.1) we get for the total Stokes drift (for derivation see Svendsen (1984 b))

$$Q_s = c \left(\frac{H}{h}\right)^2 \left(B_0 + \frac{A}{H^2} \frac{h}{L}\right) d_{tr} + O\left(\left(\frac{\eta^3}{h}\right), \ldots\right) \tag{3.3}$$

In this expression L is the "wave length" defined as $c(x)T$,

$$B_0 \equiv \overline{(\eta/H)^2} \tag{3.4}$$

and A is the area in the vertical plane of the surface roller (see Fig. 4).

Measurements of A is only available for deep water breaking behind a submerged hydofoil (Duncan, 1981) where it was found that

$$A \approx 0.9 \, H^2 \tag{3.5}$$

With no net mass (or volume) flux in the wave we also find the mean velocity U_m in the region below wave trough to be given by

$$U_m = - \frac{Q_s}{d_{tr}} \tag{3.6}$$

where d_{tr} is the water depth under the wave trough. With these results we have ensured the conservation of mass in the wave-current motion considered.

The equation of conservation of (horizontal) momentum is used on the form

$$\frac{\partial u}{\partial t} + \frac{\partial u^2}{\partial x} + \frac{\partial uw}{\partial z} = - \frac{1}{\rho} \frac{\partial p}{\partial x} \tag{3.7}$$

where viscous terms have been neglected. The balance described in Section 2 between three contributions then results in the following relation

$$\frac{\partial \overline{u^2}}{\partial x} = - g \frac{\partial b}{\partial x} - \frac{1}{\rho} \frac{\partial \bar{\tau}}{\partial z} \tag{3.8}$$

which is the time averaged momentum equation for a fluid particle. $\bar{\tau}$ is the turbulent shear stress and u the turbulent mean velocity. (3.8) only applies below the level of the wave trough u may be devided into a wave part u_w (with $\bar{u}_w = 0$) and the undertow component U. It can then be shown that consistent with assumptions already introduced we have

$$\overline{u_w^2} >> U^2 \tag{3.9}$$

so that (3.8) may be written as

$$\frac{1}{\rho}\frac{\partial\bar{\tau}}{\partial z} = \frac{\partial}{\partial x}\left(\overline{u_w^2} + gb\right) \tag{3.10}$$

The turbulent shear stress τ is described by an eddy viscosity ν_t such that

$$\tau = \rho\,\nu_t\,\frac{\partial(u_w + U)}{\partial z} \tag{3.11}$$

This is time averaged and we invoke that u_w to the first approximation can be assumed independent of z. Then we get

$$\bar{\tau} = \overline{\nu_t(t)\,\frac{\partial(u_w + U)}{\partial z}} = \overline{\nu_t(t)\,\frac{\partial U}{\partial z}} = \overline{\nu_t(t)}\,\frac{\partial U}{\partial z} \tag{3.12}$$

which means we can apply the time averaged value for ν_t. Then (3.10) can be solved directly which yields

$$U(z) = \alpha_1(x)\int\frac{z}{\nu_t(z)}\,dz + \beta_1(x)\int\frac{dz}{\nu_t(z)} + \gamma(x) \tag{3.13}$$

where

$$\alpha_1(x) = \frac{\partial}{\partial x}\left(\overline{u_w^2} + gb\right) \tag{3.13}$$

and β_1 and γ are arbitrary integration functions to be determined by the boundary conditions.

Discussion of boundary conditions

To determine β_1 and γ_1 we need two conditions.

One seems fairly obvious: that the total volume flux represented by the undertow must equal Q_s. This can also be expressed as: the mean value of U(z) between trough and bottom must be U_m, that is

$$\int_{-h_0}^{\eta_{tr}} U(z)dz = U_m\,d_{tr} \tag{3.14}$$

As the second condition it will be natural to use the boundary value for U at the bottom. To do that properly, however, we must recall that at the bottom we have an oscillating boundary layer which averaged over time shows a steady streaming. Thus a consistent choice at this boundary will be either to use as the boundary condition the steady streaming velocity U_b at the top of the oscillatory boundary layer - and neglect the thickness of that layer so that $U = U_b$ applies at $z = -h_0$ — or to include the boundary layer in the solution. The latter necessitates that the boundary layer solution is carried to second order in the perturbation expansion.

Some aspects of this problem is discussed further in section 4 but for the time being it suffice to let

$$U(z) = U_b \quad \text{for} \quad z = -h_0 \tag{3.15}$$

It may be worth briefly to examine some other possible boundary conditions for U(z).

One possibility is to replace (3.14) by a boundary condition at the trough level $z = \eta_{tr}$ where a proper description of the turbulence can yield a value for $\overline{\tau}$ i.e. a condition on $\partial U/\partial z$.

When using the shear stresses at trough level as a boundary condition it becomes necessary to analyse the magnitude of the $\partial\overline{uw}/dz$-term in (3.6) (u and w being turbulent mean velocities) relative to the turbulent contributions to $\overline{\tau}$, and that requires a far more detailed description of the wave motion. The $\overline{uw}$-term also includes the convective accelerations caused by the decrease in wave height as the water depth decreases. This will cause Q_s to decrease shorewards giving a vertical flow downwards proportional (at trough level) to $\partial Q_S/\partial x$. The effect represents an enhancement of the horizontal shear stresses. In the present very crude model this effect has been considered included in ν_t but would be necessary elements in a more detailed model.

Dally (1980) and Börekci (1982) used both (3.14) and a condition for $\overline{\tau}$ ($z = \eta_{tr}$) and considered in addition the flow between trough and crest. In combination with sinusoidal waves (which they used) this is of limited relevance.

Solutions for two ν_t-distributions

The simplest possible evaluation of (3.13) is for ν_t = const. Using the boundary conditions (3.14) and (3.15) thus yields

$$\frac{U(y)-U_b}{c} = \frac{1}{2}\frac{\alpha d_{tr}^2}{c}\left(\frac{y}{d_{tr}}\right)^2 + 2\left(\frac{U_m - U_b}{c} - \frac{1}{3}\frac{\alpha d_{tr}^2}{c}\right)\frac{y}{d_{tr}} \qquad (3.16)$$

where $y = z + h$ is the distance from the bottom and

$$\alpha \equiv \frac{\alpha_1}{\nu_t} \qquad (3.17)$$

Our knowledge, however, of the turbulence generated by the breakers indicates that it spreads downwards from the surface while decaying. Hence ν_t can be expected to decrease with distance from the surface. To model this we may use a ν_t decreasing exponentially downwards, i.e.

$$\nu_t = Ne^{a(z-\eta_{tr})} \qquad (3.18)$$

With the boundary conditions described above this yields the solution

$$U(z) = -\left(\frac{A_1}{c} + \frac{\alpha_1}{ca^2N_0}ay\right)e^{-ay} + \frac{\gamma}{c} \qquad (3.19)$$

where

$$A_1 = \frac{U_m - U_b}{M_1} - \frac{\alpha_1}{a^2N_0}\left(1 + ad_{tr} - \frac{ad_{tr}}{M_1}\right)$$

$$M_1 = \left(e^{-adtr} - 1 + ad_{tr}\right)/ad_{tr}$$

$$\gamma = U_b + A_1 \; ; \; N_0 = Ne^{-ad_{tr}}$$

4. THE EFFECT OF THE PRESSURE GRADIENT ON THE BOTTOM BOUNDARY LAYER.

The relatively strong mean pressure gradient created by the set-up also changes the momentum balance in the bottom boundary layer. The equation for the mean flow may again be derived from (3.7) but using somewhat different approximations. As before we neglect the effect of the sloping bottom. A perturbation expansion is introduced by

$$u = u^{(1)} + u^{(2)} + \ldots,\ w = w^{(1)} + w^{(2)} + \ldots;\ p = p^{(1)} + p^{(2)} + \ldots;$$

After averagering over a wave period and substitution of an eddy viscosity description for τ based on a boundary layer viscosity ν_{tb} this yields for the second order approximation

$$\frac{\partial}{\partial z}\left(\nu_{tb}\ \frac{\partial \overline{u^{(2)}}}{\partial z}\right) = \frac{\partial}{\partial z}\left(\overline{u^{(1)} w^{(1)}}\right) + \frac{\partial}{\partial x}\left(\overline{u^{(1)^2}} + gb\right) \tag{4.1}$$

Here $u^{(2)}$ represents the combined undertow and steady streaming in the boundary layer.

This is the equation describing the steady streaming in the bottom boundary layer. The first right term is the usual driving term for this flow (see e.g. Louguet Higgins 1953 , 1957). This term tends to zero as we move away from the bottom, and we see that apart from this term the equation is almost the same as (3.8) describing the undertow. The additional differences being that the oscillatory component $u^{(1)}$ is here $u^{(1)}(z)$ and ν_{tb} will in general be different from ν_t for the undertow.

A similar equation (but with some terms included representing the effect of the sloping bottom) was derived by Börekci (1982), and the peristaltic pumping studied by Longuet-Higgins (1983) leads to an equation without the $\overline{u^{(1)^2}}$-term. The orders of magnitude of the contributions to this momentum balance was discussed by Longuet-Higgins (1983).

Equation (4.1) may in fact be solved directly. For ν_{tb} = constant the solution may be written

$$\overline{u^{(2)}} = \frac{1}{\nu_{tb}} \iint \frac{\partial}{\partial x} \overline{u^{(1)^2}}(\xi)\, d\xi\, dz + \frac{g}{\nu_{tb}} \frac{db}{dx}\left(\frac{1}{2} z^2 + C_1 z + C_2\right) + u_s(z) \tag{4.2}$$

where u_s is the steady streaming without the pressure gradient and with $\frac{\partial}{\partial x} \overline{u^{(1)^2}} = 0$. Also for variable ν_{tb} is the solution straightforward, however.

The boundary conditions to be satisfied by (4.2) is that at $z = -h$ we have $\overline{u^{(2)}} = 0$ and at the upper edge of the boundary layer $\overline{u^{(2)}}$ approaches the undertow velocity U.

The solution used by Svendsen (1984b) corresponds to assuming the boundary layer infinitely thin and letting $\overline{u^{(2)}} = U_b = u_s$ at $z = -h$. We see that in (4.2) this corresponds to neglecting the first two terms inside the boundary layer.

Equation (4.2) also shows, however, that if ν_{tb} is small in comparison with ν_{tb} between bottom and trough these terms may become far more important. Comparison of the eddy viscosities ν_t found for turbulent

bores by Madsen & Svendsen (1983) with the eddy viscosities in an oscillatory boundary layer corresponding to the wave friction factors determined by Jonsson & Carlsen (1976) indicates that ν_t may be significantly larger than ν_{tb}. Further analysis is needed of this question, and also of the boundary layer under breaking waves rather than ordinary sine waves.

Using, however, a seemingly conservative estimate of ν_{tb} which is 0.2 times a typical value of ν_t in the region between trough and bottom, and constant over the boundary layer, then we get a mean velocity $u^{(2)}$ at $z = \delta$ ($\delta \equiv (2\nu_{tb}/\omega)^{\frac{1}{2}}$) which on a slope $h_x = 1/34$ is of the same order of magnitude as U_{bs} given by linear theory but of opposite sign. In other words: in the outer part of the bottom boundary layer the steady streaming is likely to be strongly seawards oriented. As it will be seen this result conforms well to the measurements presented in section 7. In the absence, however, of more precise information about this point we have chosen in the comparison with the measurements to show the effect which different values of U_b have on the undertow profile. This is done by showing theoretical results corresponding to U_b-values between + and - U_{bs} where U_{bs} is the (Eulerian) value from linear wave theory, i.e. $U_{bs} = 3/16\ c(H/h)^2$.

5. EXPERIMENTAL SET-UP

The experiments are carried out in a flume 32 m long, 60 cm wide, with a plane beach sloping 1:34.26 (see Fig. 5).

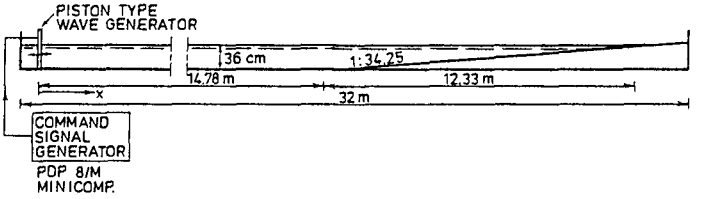

Fig. 5. Experimental set-up.

The motion of the piston type wave generator is controlled by a PDP 8 minicomputer, which generates a command signal of the form

$$\xi = e_1 \sin \omega t + e_2 \sin (2\omega t + \beta)$$

(Buhr Hansen, and Svendsen, 1974).

The water depth in front of the sloping beach is 36 cm, the wave period T = 2s, and the wave height H = 12 cm. To obtain a stable test situation in the wave flume waves were generated for at least 20 min. before any recordings were taken.

The particle velocities are measured using a bi-directional micropropeller current meter described in Basco et al, 1982. (see Fig. 6). However, for the undertow measurements special data logging and data-processing programmes were designed.

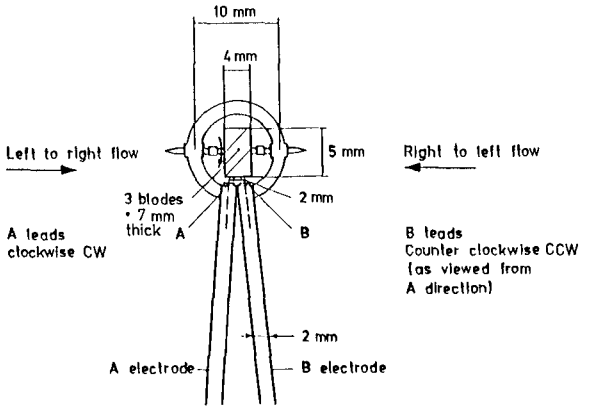

Fig. 5 Schematic illustration of the bi-directional, micro-propeller current meter showing the propeller, mounting, frame, and double electrodes to sense the blade passage for electronic interpretation. (From Basco et al. 1982).

The principle of operation of the current meter is that the propeller blades generate electric pulses when passing either of the electrodes A and B. The speed is determined directly from the length of the time interval between consecutive passages of the same electrode and the direction from the "position" of the pulse from the other electrode recorded in the same time interval.

The propeller is 5 mm diameter with 3 blades equivalent to approximately 5.2 mm peripheral distance between the blades. The propeller blade angle is 45° and the distance between the electrodes is 2 mm.

The time interval between consecutive pulses from one electrode varies from about 200 ms for velocities of 5 cm/s (about the lowest steady flow velocity that may be recorded) to about 15 ms for velocities of 50 cm/s (about the highest velocity observed in these experiments).

The datalogging programme run on a PDP 8/e minicomputer is designed to detect and store both the time of occurrence of pulses from the electrodes (accuracy 1/10 ms) and electrode identification. Notice that it is the leading edge of the pulses that is detected. Simultaneously the analog signal from a wave height meter and the analog output signal from the micro-propeller current meter are sampled. It is important to notice that the samples are triggered by the propeller blade pulses and consequently are unevenly spaced in time.

The analog current meter signal, however, is only used as support in the judging of the velocities calculated from the digital recordings. The reason is, that in oscillating flow - as in the present experiments - the online dataprocessing used to convert the propeller pulses to an analog signal yields a distorted velocity history because the output will always be the mean velocity recorded over the previous time interval, and the correct sign of the output may be delayed further.

The off line data processing programme is designed to convert all time intervals between two consecutive pulses from the same electrode

into water velocities. The speed is inverse proportional to the recorded time intervals (AA and BB respectively in Fig. 7).

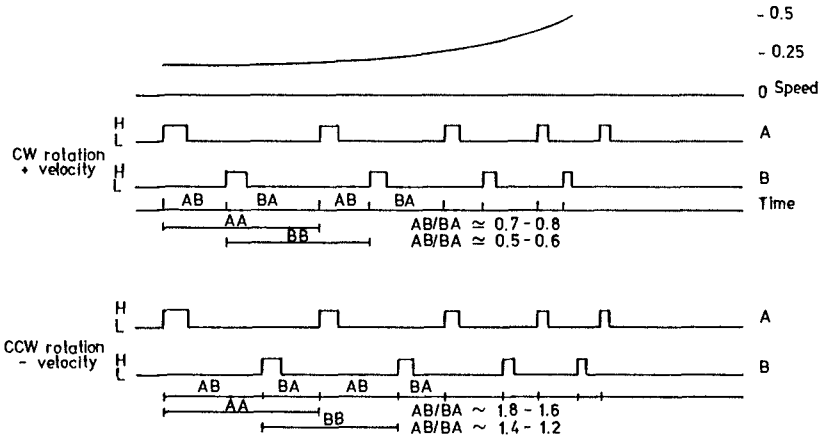

Fig. 7. Timing diagram for propeller pulses under accelerating flow. (In the case of decelerating flow the AB/BA ratios indicated for AA will be valid for BB and vice versa).

The timing diagram in Fig. 7 further shows that the position of the B-pulse between two A-pulses and vice versa yields the sign (or direction) of the velocity: i.e. AB/BA ~ .62 represents positive and AB/BA ~ 1.6 negative velocities under constant speed. However, these well defined AB/BA ratios are found only when the propeller is running at a constant speed. In the case of accelerating/decelerating flow the AB/BA ratio may change considerably. The data processing programme is through a trial-and-error method found to yield the most reliable results when in the computer program we use AB/BA > 1.3 in the AA case and 1.15 in the BB case to determine negative velocities.

When measuring in oscillating flow a special problem arises when the velocities are changing sign(the propeller changes rotational direction), and for some time the velocity remains below the minimum velocity that keeps the propeller running.

When the propeller changes rotational direction it may be observed through the registration of two consecutive pulses from one electrode without any pulse from the other electrode in the same period of time. In this case the velocity is set to zero for this period of time. However, the pulses have a width which is not negligible, and the change in rotational direction will in some cases take place while a pulse is High, and the changing direction of the flow is "only" detected as a sign shift of the calculated velocities. This causes some inaccuracy in the calculated velocity just after a sign shift, but occurs only when the velocities are small. When the velocities are changing rapidly, as it is the case around zero velocity, furthermore, the determination of the correct sign is uncertain. Around zero velocity a number of

obviously erroneous signs are observed.

Both these errors are of minor importance for the determination of the net velocity over the wave period, which is the result we are aiming at here.

Due to the presence of air bubbles in the water - and may be for other reasons as well - a few pulses are not detected by the computer. In the experiments this error occurred with a frequence of 2-4 per 1000 pulses. When appearing during a period of time with considerable velocities (> 10 cm/s) it is corrected by the off-line processing programme. This programme also corrects single velocity values which have been assigned an obviously wrong sign when compared to preceding and following values both > 10 cm/s.

It may be noticed that there is a time lag between the calculated velocities and the recorded surface elevations.

As the velocity measuring method is giving only mean velocities over the time intervals AA and BB respectively it is assumed that the measured velocities are representing the actual velocity in the middle of each time interval. The recorded analog signal from the wave height meter, however, corresponds to the instants of the propeller pulses, and the time series is consequently different from that of the velocities.

Each test comprises 2960 samples equivalent to a recording period in the range of 45 sec (22 wave periods) to 77 sec (38 wave periods).

6. DETERMINATION OF NET VELOCITIES AND WAVE DATA

For each test the two simultaneously recorded time series for horizontal particle velocities and surface elevations are analysed independently.

In both time series the individual waves in the recordings are separated through the determination of the zero-up-crossings of the signals and for each individual wave the time average value over the wave period as well as the RMS, maximum and minimum values are calculated. In turn these figures are averaged over the total number of waves included in the time series for each test. Fig. 8 contains a summery of all test results. (Only the experiments in the surf zone are analysed further in this paper).

Each test is associated with a specific horizontal position in the wave flume and a specific depth - or height over the bottom - where the velocity meter is located.

As all tests are performed using the same wave input, the recordings of surface elevations at any of the 6 horizontal positions are repeated a number of times, yielding a possibility of judging the inaccuracies involved in the recordings.

In the surf zone the variations in all surface wave data, e.g. η_{RMS}, H and b, from wave to wave are very significant. Reliable results can consequently only be obtained when the results are averaged over a great number of waves. In these experiments, where one test run comprises 22 to 38 waves, all results are averaged over the total number of waves recorded.

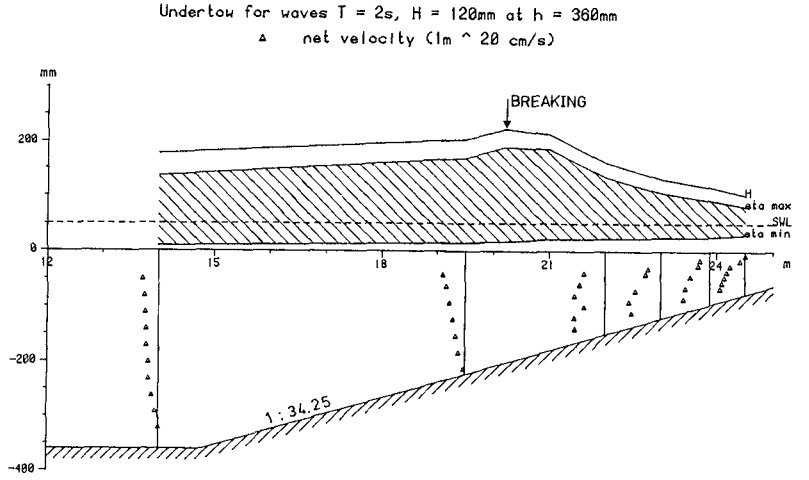

Fig. 8. *Summary of test results.*

The resulting averaged η_{RMS} values are from test to test reproduced with a standard deviation below 1 mm. Just after breaking the averaged wave heights H are similarly reproduced with standard deviations about 4 mm. Before breaking, and further into the surf zone, however, the standard deviations on H are much smaller (about 1 mm). Similarly the set-down/set-up values are associated with standard deviations of .5-1 mm.

The analysis of the particle velocity measurements clearly reveals the very irregular and strongly turbulent velocity pattern expected after wave breaking. The resulting average net velocities at different positions and depths are given in fig. 8. Each of these net velocities are the averaged values over the 22 to 38 waves included in one test. The single wave net velocities reveal considerable variations, and the average value is within each test associated with a standard deviation about 10 mm/s outside the breaking point and 30-45 mm/s in the surf zone. Nevertheless, two of the tests in the surf zone have been repeated 4 times each, and from test to test the averaged net velocities vary only about ± 5 mm/s.

7. COMPARISON WITH MEASUREMENTS

To obtain numerical results from (3.16) or (3.19) for comparison with the measurements we first realize that these solutions have the parameters

$$\nu_t = \text{const.} \quad : \quad \frac{\alpha\, d_{tr}^2}{c}, \quad \frac{U_m - U_b}{c}$$

$$\nu_t = Ne^{az} \quad : \quad \frac{\alpha(\eta_{tr}) \cdot d_{tr}^2}{c} = \frac{\alpha_1\, d_{tr}^2}{cN}, \quad ad_{tr}, \quad \frac{U_m - U_b}{c}$$

In the following we only consider the latter of the two models.

If we consider h as the known quantity in stead of d_{tr} this adds another parameter d_{tr}/h to the list.

Here the value of U_b/c has been discussed in Section 4.

For $\alpha_1 = \partial/\partial x(\overline{u_w^2} + gb)$ we find with $\frac{H}{h} \sim 0.6$

$$\frac{\partial}{\partial x}\overline{u_w^2} \approx \frac{\partial}{\partial x} c^2 \left(\frac{\eta}{h}\right)^2 \approx B_0 \left(\frac{H}{h}\right)^2 g\, h_x \approx 0.027\, g h_x$$

$$\frac{\partial}{\partial x} gb \approx g\ 0.18 \cdot \frac{H}{h} h_x \approx 0.11\, g h_x$$

so that $\alpha_1 \approx 0.14\, g\, h_x$. The turbulence model used by Madsen & Svendsen (1983) yields ν_t-values ≈ 0.005-0.010 ch depending on the characteristic parameters used. Thus we get for $\alpha_1 d_{tr}^2 / c\ \nu_t$

$$\frac{\alpha_1 d_{tr}^2}{c\nu_t} \approx \frac{\alpha_1 h^2}{c\nu_t} \approx 14 - 27\, h_x$$

In the present experiments this means

$$A = \frac{\alpha_1 h^2}{c\, \nu_t} = 0.4 - 0.8$$

Svendsen (1984b) used A = 0.4 for Stive and Wind's 1982 experiments.

In the comparison with experiments we find that A = 0.2 and 0.4 yield the best agreement (Fig. 9) but have shown a comparison including A = 1.0 (Fig 10) which illustrates that the velocity profile is quite sensitive to the value of A. Clearly further investigations of this problem would be desirable.

The parameter ad_{tr} represents the decay of the turbulence downwards from the trough level. $ad_{tr} = 1$ represents a bottom value of ν_t which is 37% of the surface value, and $ad_{tr} = 2$ similarly represent a reduction to 14% of the surface value.

Figs. 9 and 10 show comparison with the measurements described in section 5 and 6.

A number of observations can be made from the Figs. 9 and 10:

a) The depth averaged value U_m of the undertow determined from the shoreward mass flux by (3.6) is generally in good agreement with the measured values

b) The measurements going closer to the bottom indicates more clearly than those by Stive & Wind (used by Svendsen (1984b)) that the steady streaming in the boundary layer is likely to be in the seaward direction, and with $U_b = - U_{bs}$ the theoretical results agree quite well with the measurements.

c) The results appear to be very sensitive to the value of A, A = 1.0 being obviously too large. On the other hand the value of ad_{tr} has been found not to influence the theoretical results nearly as much.

Considering the relatively simple model and the uncertainties

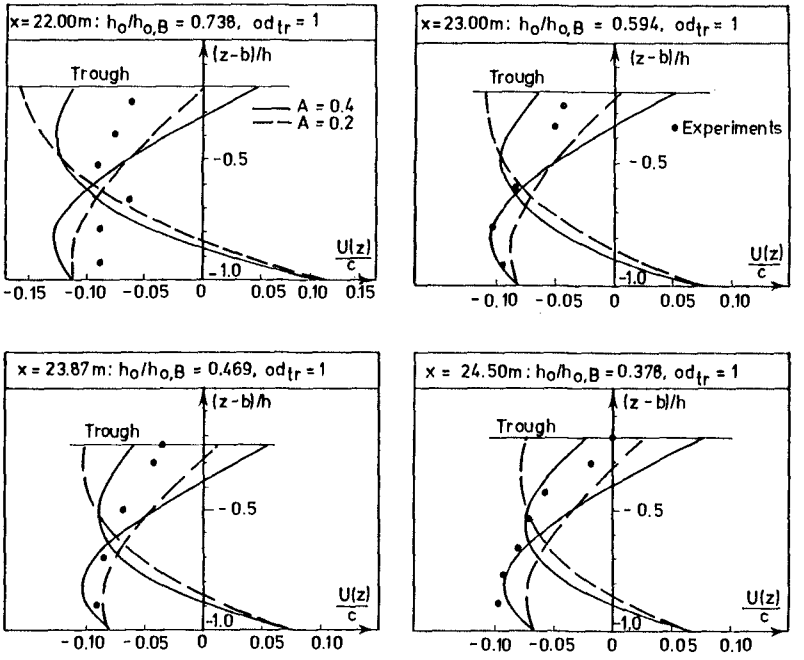

Fig. 9. *Comparison between experiments and eq. (3.19) with* $U_b = \pm U_{bs}$ *and* $A = 0.2$ *and* 0.4.

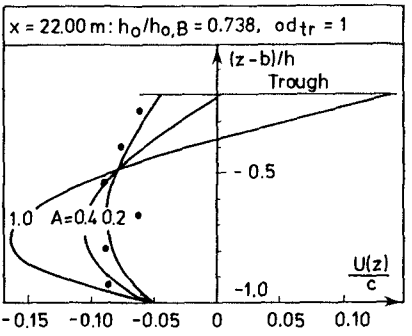

Fig. 10. Comparison between experiments and eq. (3.19) with $A = 0.2$, 0.4 *and* 1.0.

regarding at least the two important parameters U_b and ν_t the agreement must be considered quite satisfactory.

The large seaward velocities near the bottom are considered of significant importance for the erosion of coastlines under storm conditions.

From (3.10) we see that the shear stress τ varies linearly with z irrespective of ν_t. We have for τ

$$\bar{\tau} = \rho \nu_t \frac{\partial U}{\partial z} = \rho(\alpha_1 z + \beta_1)$$

The eddy viscosity model also implies that the maximum value of U corresponds to $\bar{\tau} = 0$. In combination with the linear $\bar{\tau}$-variation this means that the relative height $y0/d_{tr}$ above the bottom of U_{max} indicates the magnitude of $\bar{\tau}_b$ relative to the total shear stress variation. Thus the measurements in Figs. 9 and 10 corresponds to very small $\bar{\tau}_b$-values, whereas the measurements by Stive & Wind (1980) used by Svendsen (1984b) seem to indicate larger $\bar{\tau}_b$-values, though the scattering of the results and the lack of measurements sufficiently close to the bottom make a conclusion at this point uncertain.

REFERENCES

Bagnold, R.A. (1940). Beach formation by waves; some model experiments in a wave tank. J. Inst. Civ. Eng., 15, 27-52.

Basco, D.R., Ib A. Svendsen and J. Christensen (1982). Measurements with a bi-directional micro-propeller current meter, Inst. of Hydrodynamics & Hydraul. Eng. (ISVA), Tech. Univ. Denmark, Prog. Rep. 57, 25-32.

Börekci, O.S. (1982). Distribution of wave-induced momentum fluxes over depth and application within the surf-zone. Ph. D. Dissertation, Dept. Civil Eng., Univ. of Delaware.

Buhr Hansen, J. and I.A. Svendsen (1974). Laboratory generation of waves of constant form. Proc. 14th Coastal Eng. Conf., Copenhagen, chap. 17, 321-339.

Dally, W.R. (1980). A numerical model for beach profile evolution, Master's thesis, University of Delaware, Dept. of Civ. Engrg.

Duncan, J.H. (1981). An experimental investigation of breaking waves produced by a towed hydrofoil. Proc. R. Soc., London, Ser. A. 377, 331-348.

Dyhr-Nielsen, M. and Sørensen, T. (1970). Sand transport phenomenona on coasts with bars. Proc. 12th Coastal Eng. Conf., Washington, D.C., Chap. 54, 855-866.

Guza, R.T. (1984). Private communication.

Johnson, D.W. (1919). Shore processes and Shore line Development. Facsimile reproduction 1972, Hafner Publishing Company, New York.

Longuet-Higgins, M.S. (1953). Mass transport in gravity waves. Philos. Trans. R. Soc. London, Ser. A, 245, 535-581.

Longuet-Higgins, M.S. (1957). The mechanics of the boundary layer near the bottom in a progressive wave. Proc. 6th Coast. Engrg. Conf., Chapt. 10, 184-193.

Longuet-Higgins, M.S. (1983). Peristaltic pumping in water waves. J. Fluid Mech., 137, 393-409.

Madsen, P.A. & I.A. Svendsen (1983). Turbulent bores and hydraulic jumps J. Fluid Mech., 129, 1-25.

Stive, M.J.F., and Wind, H.G. (1982). A study of radiation stress and set-up in the near-shore region. Coastal Eng., 6, 1-25.

Svendsen, I. A. (1984a). Wave heights and set-up in a surf zone. Coastal Engineering, 8, 4, 303-329.

Svendsen, I.A. (1984b). Mass flux and undertow in a surf zone. Coastal Engineering, 8, 4, 347-365.